



PERGAMON

Available online at www.sciencedirect.com

SCIENCE @ DIRECT®

Planetary and Space Science 50 (2002) 915–927

Planetary
and
Space Science

www.elsevier.com/locate/pss

Ultraviolet radiation on the surface of Mars and the Beagle 2 UV sensor

M.R. Patel^{a,*}, J.C. Zarnecki^a, D.C. Catling^b

^aPlanetary and Space Sciences Research Institute, The Open University, Walton Hall, Milton Keynes, MK7 6AA, UK

^bDepartment Atmospheric Sciences and Astrobiology Program, Box 351640, University of Washington, Seattle, WA 98195, USA

Abstract

In this paper a simple radiative transfer model for the transmission of UV to the surface of Mars is presented for the wavelength range 190–410 nm. The model accounts for the variable presence of dust aerosols in the martian atmosphere and its effects upon direct and diffuse irradiance. A range of situations is presented, including variations in orbital position, latitude, time of day, dust loading and ozone presence. High dust loading is seen to have an inverting effect on direct/diffuse transmission ratios, with a significant amount of illumination still being provided even at high optical depths typical of dust storms. Diffuse transmission is also observed as the primary component close to sunrise and sunset as expected. An ozone absorption feature is seen for high-latitude northern winter cases, offering limited shielding centred around 250 nm in the biologically damaging region of the UV spectrum.

The use of the model is then discussed in the role of designing and developing the Beagle 2 UV sensor, an instrument to measure the surface UV flux between 200 and 400 nm and set to land on the surface of Mars in 2003. The model is used to determine flux levels and spectral regions of particular interest, leading to a detailed instrument design and specification.

© 2002 Elsevier Science Ltd. All rights reserved.

Keywords: Mars; UV; Dust; Atmosphere; Beagle 2

1. Introduction

Ultraviolet (UV) radiation has wavelengths between that of visible violet light (400 nm) and X-rays (4 nm). However, the UV flux on the surface of Mars is significant only in the near (300–400 nm) and far (200–300 nm) UV because of absorption and scattering in the martian atmosphere. Ultraviolet light forms a relatively small part of the solar flux (typically < 5% of the solar constant), yet its effects are highly significant both in the question of life and the issue of atmospheric photochemical interactions. The UV environment at the surface of Mars helps to determine biological survivability. Short-wave UV-C (200–280 nm) can be extremely damaging to biological organisms, and must be considered in any extraterrestrial situation when looking for the possibility of sustaining life (Cockell et al., 2000). Mars shares many attributes with Earth (Lodders and Fegley Jr., 1998) making it one of the more probable places for the existence of extraterrestrial life in the Solar System.

Previous experimental investigation of the UV environment on Mars has been solely in the form of remote

observation, with no in situ investigations of the surface flux to date. Remote sensing by the UV spectrometer instruments on the Mariner 7 and 9 probes has been carried out (Barth and Hord, 1971; Barth et al., 1973), followed by Phobos-2 observations in the UV-A (> 315 nm) region (Moroz et al., 1993; Wuttke et al., 1997). Hubble Space Telescope observations have also been conducted (James et al., 1994), yet these observations all require an accurate knowledge of surface and atmospheric reflectance properties in order to determine the flux that reaches the surface. In situ observations are thus required to give ground truths to these remote observations. Also, remote sensing is limited by spatial resolution in determining the effect of specific small-scale localised phenomena on the UV flux, for which direct surface observation is necessary.

The deleterious effects of short-wave UV-C have been demonstrated experimentally through exposure of *Bacillus subtilis* spores to the extraterrestrial solar spectrum (Horneck, 1993). A high enough dosage of UV radiation has the potential to sterilise any surface layer bearing microorganisms. The thin CO₂ atmosphere of Mars does not contain a global ozone layer as on Earth, which blocks out a substantial part of the biologically damaging component of UV. The issue of survivability of life in the UV environment at the surface of Mars has been addressed previously using

* Corresponding author. Tel.: +44-1908-659598; fax: +44-1908-858022.

E-mail address: m.r.patel@open.ac.uk (M.R. Patel).

theoretical and experimental techniques (Sagan and Pollack, 1974; Cockell et al., 2000; Mancinelli and Klovstad, 2000). Modelling techniques help gain an understanding of the surface environment in a variety of situations. Previously published work (Kuhn and Atreya, 1979; Cockell et al., 2000) has dealt with the issue of UV flux at the martian surface. The model described in this paper is constructed in a similar manner to that briefly discussed by Cockell et al. (2000) using the same radiative transfer approximation method. Presented here is a model with updated dust optical properties based on recent modelling of previous observations, with new gas absorption coefficients appropriate to the martian atmosphere. The optical properties of martian dust have been investigated in situ by the Viking and Pathfinder imagers, but have not been well constrained in the UV region of the spectrum. Modelling of the surface environment is also used to set operating parameters of the UV instrumentation currently being prepared for the Beagle 2 lander in 2003, and also to prepare for interpretation of results to be returned by this instrument.

2. UV surface flux model

2.1. Model inputs

The primary input parameters to the model are: local surface pressure, latitude, areocentric longitude (L_s , which is a measure of orbital position or season), time of day, O_3 abundance and dust optical depth (water vapour and water ice clouds are not considered here). To model the UV flux at any point over the martian surface at any time, input factors such as L_s , latitude and time of day are required to define position of the Sun in the sky. These factors define the geometry while the remaining inputs serve to describe the atmospheric conditions. For the input parameter of dust optical depth, the reference wavelength is taken to be 670 nm where the measured optical depth is nearly equal to the optical depth value averaged over the solar spectrum (Pollack et al., 1979). As a primary input factor to the model (set by L_s , latitude and time of day) the solar flux at any point in the martian orbit was explicitly calculated. Mars' relatively high eccentricity (compared to the Earth) causes significant variation in solar insolation from perihelion to aphelion. The flux at any point in the martian orbit can be calculated by inverse square law scaling from the solar flux at 1 AU, as measured by the SUSIM UARS instrument on ATLAS-1 (Cebula et al., 1996, Floyd et al., 1999). The Sun–Mars distance r at any point in the martian orbit can be determined from the areocentric longitude by

$$r = \frac{d(1 - e^2)}{1 + e \cos(L_s - L_s^p)}, \quad (1)$$

where d = mean Mars distance (1.52 AU), e = Mars eccentricity (0.0934) and L_s^p = longitude of perihelion (250°). Knowing the flux at any orbital point, the input flux (F_0) to

the top of the atmosphere is then found by consideration of the solar zenith angle calculated from the input parameters

$$F_0 = \mu F_{1.52} \left(\frac{d^2}{r^2} \right), \quad (2)$$

where $F_{1.52}$ = flux at 1.52 AU (the mean Mars orbital distance), $\mu = \cos z$, where z is the solar zenith angle given by

$$\cos z = \sin \theta \sin \delta + \cos \theta \cos \delta \cos h, \quad (3)$$

where θ = latitude, δ = solar declination and h = hour angle. Solar declination is found using $\sin \delta = \sin \varepsilon \sin L_s$ (where ε is the martian obliquity, 25.2°), and the hour angle h is defined as

$$h = \frac{2\pi t}{P}, \quad (4)$$

where $P = 88775$ s (the martian solar day), and t = time in seconds measured from local noon. Substitution of the above into Eq. (2) gives

$$F_0 = F_{1.52} \left[\sin \theta \sin \varepsilon \sin L_s + \cos \theta \cos \left(\frac{2\pi t}{P} \right) \times (1 - \sin^2 \varepsilon \sin^2 L_s)^{1/2} \right] \left[\frac{1 + e \cos(L_s - L_s^p)}{1 - e^2} \right]^2 \quad (5)$$

i.e. a term which describes the top of atmosphere flux for Mars in terms of the inputs θ , L_s and t over any part of the martian orbit, viewed from any point at the surface at any time of day.

2.2. Direct flux calculation

In cases of relatively dusty atmospheres, such as is encountered on Mars, there are two distinct processes which govern the passage of radiation to the surface: direct attenuation and diffuse scattering/absorption effects. It should be noted that no altitude dependence of atmospheric species is considered here since only surface irradiance is addressed, and therefore only integrated column densities for atmospheric constituents are considered. Thus, the solar UV flux at the surface can be separated into two components, direct and diffuse flux:

$$F_{\text{surface}} = F_{\text{direct}} + F_{\text{diffuse}}. \quad (6)$$

First the amount of direct sunlight transmitted through the atmosphere was calculated (F_{direct}). Beer's Law attenuation was used as follows:

$$\begin{aligned} F_{\text{direct}}(\lambda) &= F_0 e^{-\tau(\lambda)/\mu} \\ &= F_0 e^{-(\tau_{\text{gs}}(\lambda) + \tau_{\text{ga}}(\lambda) + \tau_{\text{dust}}(\lambda))/\mu} \\ &= F_0 e^{-(n\sigma_{\text{gs}}(\lambda) + n\sigma_{\text{ga}}(\lambda) + \tau_{\text{dust}}(\lambda))/\mu}, \end{aligned} \quad (7)$$

where τ is the total optical depth of the atmospheric column. τ_{gs} and τ_{ga} are the gaseous optical depths due to scattering and absorption, respectively. n is the column abundance of the absorbing gas species, σ_{gs} is the

Table 1
The martian atmospheric composition

Martian atmospheric composition	
CO ₂	95.32%
N ₂	2.7%
Ar	1.6%
O ₂	0.13%
CO	0.07
O ₃	Variable
H ₂ O	0.03 (variable)
Ne	2.5 ppm
Kr	0.3 ppm
Xe	0.08 ppm

gas scattering cross-section and σ_{ga} is the gas absorption cross-section. For the case of direct attenuation due to dust, τ_{dust} was taken as the input optical depth value scaled linearly with the extinction efficiency of the dust particles as a function of wavelength (explained later). In the case of gaseous extinction, values of n , σ_{gs} , and σ_{ga} were defined for each atmospheric constituent as a function of wavelength, to determine the interaction of incoming solar radiation with each gas species component. The scattering cross-sections for each gas were taken to be the Rayleigh cross-sections.

The martian atmosphere is primarily CO₂ with a balance of nitrogen, argon and trace species (Table 1; Owen, 1992). The only relevant absorbers in the UV are CO₂, O₂ and O₃. N₂ (the second most abundant species in the atmosphere at 2.7%) does absorb in the UV, but only at wavelengths < 100 nm. These features are never observed at the surface due to the large CO₂ shielding effect (discussed later) and as such have a negligible contribution to the spectra presented here. All other observed species also do not absorb in the UV appreciably in the wavelength range of interest and are present only as minor constituents; they therefore have no major consequence. In these cases, the absorption coefficients for these species were taken as equal to their Rayleigh scattering values. Thus, only the absorption resulting from CO₂, O₃ and O₂ was used to calculate major direct absorption effects through the atmospheric column, with other species accounted for but having negligible effects.

2.3. Gas absorption cross-sections

The absorption data of Lewis and Carver (1983) were used to define the cross-section of CO₂ in the extreme UV (120–197 nm). The cross-section of this species is required in this wavelength region as it defines the lower wavelength cutoff in the martian atmosphere, since below 190 nm the cross-section becomes increasingly larger. The work of Lewis and Carver (1983) consists of studies at 200 K, relevant to the cold martian atmospheric environment. The temperature dependence of the cross-section is non-trivial and should be accounted for properly, especially around 190 nm where significant variation is seen between 200 and 300 K. The CO₂ cross-section variation with both wavelength and

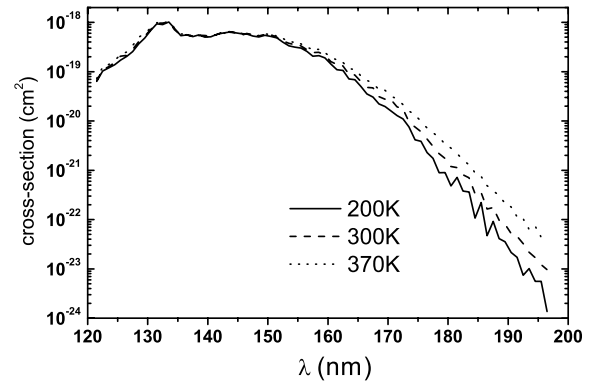


Fig. 1. The CO₂ absorption cross-section at 200 K as a function of wavelength. Also shown are cross-sections at 300 and 370 K, highlighting the temperature dependence (Lewis and Carver, 1983).

temperature can be seen in Fig. 1. Above about 200 nm, the absorption cross-section diminishes and Rayleigh scattering dominates. The predominantly CO₂ atmosphere means that even around 190 nm where the absorption cross-section is rapidly decreasing with increasing wavelength, there is still a large absorption effect due to the large column abundance. The result is a characteristic steep CO₂ transmission cutoff observed in every transmission curve near 190–200 nm.

O₂, which plays a role in the absorption of terrestrial UV, has little effect in the martian atmosphere mainly due to the difference in relative abundance. O₂ has two main absorption features in the ultraviolet region. The first are the Schumann–Runge bands, closely spaced narrow absorption features in the region 175–195 nm. These effects are never observed in martian UV spectra due to the CO₂ cutoff and as such need not be considered. The second feature is the weaker Herzberg continuum between 200 and 240 nm, where the cross-section is of the order of 10^{−23} cm². Above this, the absorption effects are negligible. The absorption data of Amoroso et al. (1996) was used for Herzberg continuum cross-section values from 200 to 240 nm, included here for completeness.

Ozone has two distinct absorption features in the 200–400 nm region; a strong absorption band centred around 250 nm in the Hartley continuum and the weaker absorption peaks in the Huggins band between 300 and 350 nm. This biologically relevant region of the UV is strongly absorbed in the terrestrial atmosphere, where O₃ is found globally in significant amounts within the stratosphere resulting in a terrestrial UV cutoff near 290 nm. On Mars, however, O₃ is far less abundant, appreciable only at high latitudes in winter and is therefore considered here as a variable factor inputted into the model. In this model, the absorption cross-sections for O₃ derived by Malicet et al. (1995) were used. Their measurements were made around 218 K, giving a closer thermal representation of the martian atmospheric environment. As can be seen in Fig. 2, the peak of the absorption occurs around 250 nm where the cross-section becomes significantly large.

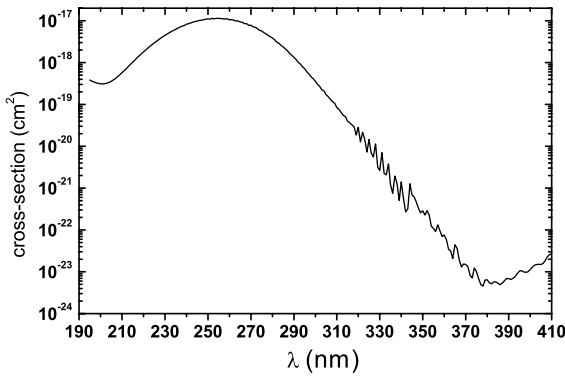


Fig. 2. The O_3 absorption cross-section as a function of wavelength at 218 K (Malicet et al., 1995).

The individual column abundance of the various gases are all set via input surface pressure, except O_3 which is inputted separately. Once the surface pressure is defined, the column abundance of the martian atmospheric species are easily determined through a knowledge of partial pressure at the surface and mean molecular mass (an assumption here is that mean molecular mass is invariant with altitude). The column abundance of each individual species was then calculated from the total atmospheric column abundance and mixing ratio of each species. The gaseous optical depth due to scattering and absorption was calculated for each species separately. This process was performed between 190 and 410 nm at 1 nm intervals for each gas. The total atmospheric optical depth for the complete atmosphere is then found by summing τ_{gs} and τ_{ga} for each gas species with τ_{dust} , then used in Eq. (7) to generate a wavelength-dependent direct flux at the surface.

2.4. Diffuse flux

The scattering and absorption properties of aerosols present in the martian atmosphere are now addressed in order to quantify the diffuse illumination at the martian surface. Aerosol abundance can rise high enough to affect significantly the surface flux through scattering processes. Here, the aerosols are treated as pure dust and effects due to the presence of ice crystals are not addressed in this version of the model. In order to understand the nature of the interaction of the dust particles with solar radiation, the optical properties of the dust need to be known at ultraviolet wavelengths and combined together with the gaseous properties to define the complete atmosphere scenario. An appropriate radiative transfer approximation is then employed to quantify the transmission through the atmosphere. The model used here to define the dust optical properties is that of Ockert-Bell et al. (1997) which combines observational information from the Viking landers and Phobos 2 spacecraft with telescopic observations to give a model of the optical properties of martian dust over the spectral

region 0.21–4.3 μm . The optical properties of relevance here are the dust single-scattering albedo ω_o (the ratio of scattered light to that scattered and absorbed per scattering event), the particle asymmetry factor g_d (a measure of the degree of forward scattering per interaction) and the extinction efficiency Q_{ext} (the ratio of the extinction cross-section to the geometric cross-section). Interpolation between data from their model was used to characterise the parameters between 190 and 400 nm shown in Fig. 3.

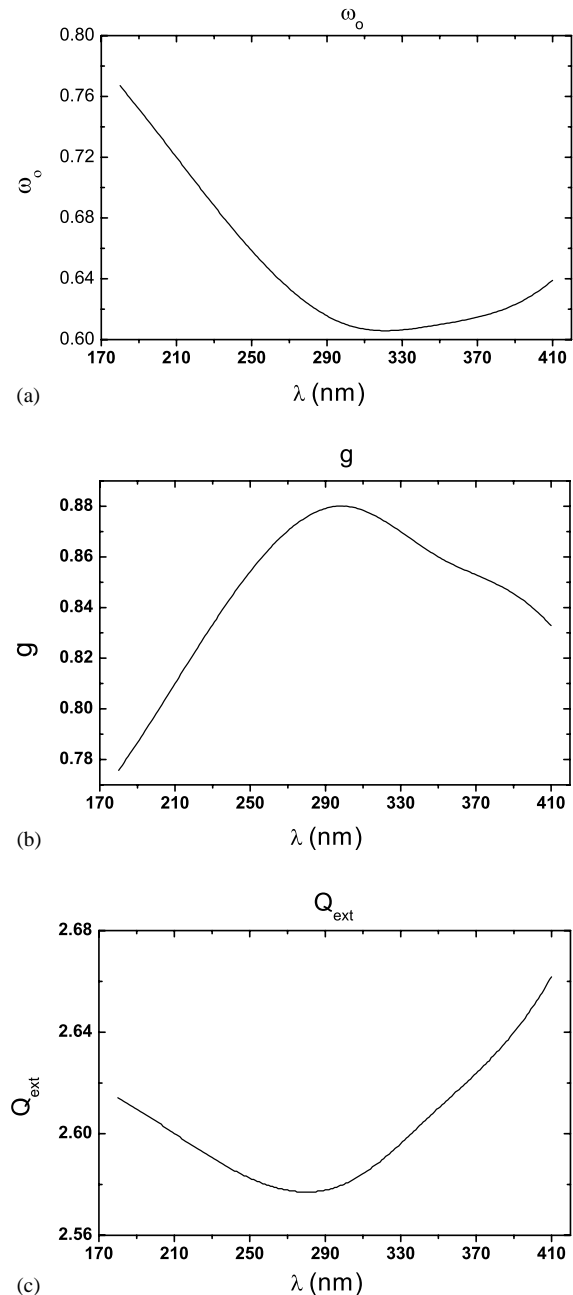


Fig. 3. The optical properties of martian dust interpolated from the data of Ockert-Bell et al. (1997): (a) shows the variation of ω_o (single-scattering albedo); (b) shows the variation of g (particle asymmetry factor) and (c) shows the variation of Q_{ext} (extinction efficiency).

2.4.1. UV dust properties

The optical properties of martian dust in the UV region remain uncertain, with relatively little work performed to date. Significant variations of the optical properties in the UV have been reported, with little agreement between different sources. Pang et al. (1976) analysed results from Mariner 9 UV spectrometer data to derive complex indices of refraction at 268 and 305 nm using Mie theory for spherical particles, with Chylek and Grams (1978) repeating the analysis using non-spherical particle theory. These studies found the dust at these wavelengths to be less absorbing than the Ockert-Bell et al. (1997) results. The opposite result is seen in Hubble Space Telescope (HST) data from Wolff et al. (1997) who used the Wide Field Planetary Camera for observations of dust storms in the Hellas and polar regions, implying a more absorbing dust in the UV region. Zureck (1978) used further complex indices of refraction from the data of Pang and Ajello (1977) to derive the optical properties ω_0 and g at wavelengths of 201, 308 and 388 nm (it should be noted here that Mie theory was used in these calculations, and this does introduce errors into the derived particle parameters in the martian case, which involves non-spherical atmospheric dust (Pollack et al., 1979) for which Mie theory is not strictly accurate). These results show an agreement with Wolff et al. (1997) for ω_0 at 201 nm, but differ towards 300 nm tending more to the value of Ockert-Bell et al. (1997), only to diverge again at 388 nm. Much more investigation from orbiting or surface instrumentation is required (contrasting the visible–IR range, which is far better defined and consistent between studies) to gain a more complete and accurate dataset. Other factors too need to be considered when addressing the UV properties of dust. The published work has been carried out at different periods of dust activity and in differing regions, and as a result one would expect variations in optical properties. Small variations in particle size distribution and complex refractive index across the martian terrain could occur, affecting the optical properties of the dust. Size distributions may for example, vary as a result of differing weathering processes or rates in different regions, resulting in different size distributions in the atmosphere. Also, for example, a small variation in a UV absorbing component which is present in only small quantities anyway (such as TiO₂ as proposed by Pang and Ajello (1977), verified by Bell III et al. (2000) through Pathfinder results) could account for a slight variation in imaginary index of refraction of the dust in different areas. Quantifying the extent to which these proposed variations have on the scattering and absorption properties is beyond the scope of this paper, and is an area which needs to be investigated. A collation of all the UV data is shown in Table 2.

The values derived from the paper by Ockert-Bell et al. (1997) however rely on whole disk spectra taken from telescopic observations (Owen and Sagan, 1972) covering a range of planetary environments including limb hazes and polar cap regions. Dust optical properties derived from these global observations and applied to specific regions are not

always completely reliable and can be a source of significant errors. Due to the limitations of available data the approach used here for martian dust optical properties is the best we can achieve at present, and this should be considered with the results. Further detailed observational work coupled with rigorous modelling is required in future to define these optical parameters more accurately.

2.4.2. Calculation of the diffuse component

For the radiative transfer approximation used in this model the single-scattering properties of the total atmospheric gas/dust mixture need to be found. The variation of the input dust optical depth (τ_{dust}) with wavelength was scaled linearly with Q_{ext} . The relative contribution of scattering and absorption to optical depth was calculated for the dust as was performed for the gaseous species in the previous section. This is achieved via consideration of the single-scattering albedo and the optical depth at each individual wavelength. Since ω_0 is defined as the ratio of scattered light to that of scattered and absorbed per single-scattering event, the product of ω_0 and τ_{dust} determines the dust scattering contribution to optical depth, τ_{ds} . The absorption component of dust optical depth τ_{da} is then simply found by subtraction of τ_{ds} from τ_{dust} .

The total contributions from gas and dust for both components (scattering and absorption) of the optical depth can then be found by

$$\tau_s = \tau_{\text{gs}} + \tau_{\text{ds}}, \quad (8)$$

$$\tau_a = \tau_{\text{ga}} + \tau_{\text{da}}, \quad (9)$$

where τ_s = total atmospheric scattering optical depth, and τ_a = total atmospheric absorption optical depth.

With these terms derived, the effective single-scattering properties of the ‘composite’ atmosphere of gases and dust can now be found. The effective single-scattering albedo ω is found by

$$\omega_{\text{eff}} = \frac{\tau_{\text{gs}} + \tau_{\text{ds}}}{\tau_{\text{gs}} + \tau_{\text{ga}} + \tau_{\text{ds}} + \tau_{\text{da}}} = \frac{\tau_s}{\tau_s + \tau_a}. \quad (10)$$

The effective asymmetry factor g for the composite atmosphere is given as the weighted sum of the individual species asymmetry factors:

$$g = \frac{(\tau_{\text{gs}} + \tau_{\text{ga}})g_{\text{gas}} + \tau_{\text{d}}g_{\text{d}}}{(\tau_{\text{gs}} + \tau_{\text{ga}}) + \tau_{\text{d}}} = \frac{\tau_{\text{d}}g_{\text{d}}}{\tau_{\text{gs}} + \tau_{\text{ga}} + \tau_{\text{d}}}, \quad (11)$$

since for Rayleigh scattering by gas molecules the gaseous asymmetry factor g_{gas} is equal to zero. The total atmospheric optical depth τ is then calculated as

$$\tau = \tau_s + \tau_a. \quad (12)$$

From here the Delta–Eddington approximation (Joseph et al., 1976; Haberle et al., 1993) which allows fast computation of the scattering process, was used to solve the

Table 2

Single-scattering properties of martian dust in the 200–400 nm region. The work of Pollack et al. (1995) is included near 500 nm to highlight the fact that some correlation is observed in the visible region, but not in the UV

λ (nm)	Ockert-Bell et al. (1997)			Wolff et al. (1997)			Zureck (1978)			Pollack et al. (1995)		
	ω_o	g	Q_{ext}	ω_o	g	Q_{ext}	ω_o	g	Q_{ext}	ω_o	g	Q_{ext}
201							0.58	0.89				
210	0.72	0.81	2.60	0.57								
300	0.61	0.88	2.58	0.57								
308							0.68	0.82				
350	0.61	0.86	2.61									
388							0.86	0.75				
400	0.63	0.84	2.65	0.63								
442							0.89	0.73				
490									0.79	0.68	2.82	
500	0.78	0.73	2.82	0.75								
550									0.84	0.66	2.89	
586							0.91	0.70				

radiative transfer equation for the transmission of solar radiation to the surface. The transmission T for the Mars atmosphere considered here can be calculated from

$$T = C_1 e^{-k\tau}(1 + P) + C_2 e^{k\tau}(1 - P) - (\alpha + \beta - 1)e^{-\tau/\mu}, \quad (13)$$

where

$$C_1 = -\frac{(1 - P)Be^{-\tau/\mu} - (\alpha + \beta)Ce^{k\tau}}{(1 + P)Ce^{k\tau} - (1 - P)De^{-k\tau}},$$

$$C_2 = \frac{(1 + P)Be^{-\tau/\mu} - (\alpha + \beta)De^{-k\tau}}{(1 + P)Ce^{k\tau} - (1 - P)De^{-k\tau}},$$

A = surface albedo,

$$B = A + (1 - A)\alpha - (1 + A)\beta,$$

$$C = (1 - A) + P(1 + A),$$

$$D = (1 - A) - P(1 + A),$$

$$k = (3(1 - \omega_{\text{eff}})(1 - g\omega_{\text{eff}}))^{1/2},$$

$$P = \frac{2}{3} \left[\frac{3(1 - \omega_{\text{eff}})}{(1 - g\omega_{\text{eff}})} \right]^{1/2},$$

$$\alpha = \frac{3}{4} \mu \omega_{\text{eff}} \left[\frac{1 + g(1 - \omega_{\text{eff}})}{1 - (\mu k)^2} \right],$$

$$\beta = \frac{1}{2} \mu \omega_{\text{eff}} \left[\frac{(1/\mu) + 3g\mu(1 - \omega_{\text{eff}})}{1 - (\mu k)^2} \right].$$

The surface albedo is taken as 0.03 unless otherwise stated. The diffuse component of irradiance can be found through subtraction of the direct component from Eq. (13). This process was performed for wavelengths between 190 and 410 nm at 1 nm intervals to yield the UV spectrum at the

surface of Mars in terms of both direct and diffuse components.

3. Model results

The model was applied to a variety of martian conditions in order to determine the variability of UV penetration. Examples are shown of diurnal, seasonal, latitudinal and dust loading variations across the martian surface. Results are consistent with those of previous investigation by Kuhn and Atreya (1979) and Cockell et al. (2000).

3.1. Varying dust case

The periods of low dust levels in the martian atmosphere tend to occur near aphelion (northern summer) in the martian orbit, with high activity and possible global dust storms occurring towards perihelion (southern summer). Typical values for the martian background haze optical depth during quiet dust activity periods range between 0.1 and 0.4 (Toigo and Richardson, 2000). The upper and lower limiting cases of this period are shown for northern summer time in Fig. 4.

As can be seen, the effect of direct attenuation is fairly insignificant, with the only noticeable absorption occurring at the CO₂ cutoff point around 190 nm. Rayleigh scattering increases towards shorter wavelengths but still has only a minor effect. In the minimum dust loading scenario ($\tau_d = 0.1$), the diffuse component is extremely low, as expected, increasing slightly for the nominal case of $\tau_d = 0.4$.

High dust loading cases on Mars create interesting effects on surface irradiance through direct and diffuse illumination due to the scattering nature of the atmospheric aerosols present. Apart from the ubiquitous background haze present throughout the year, periods of dust activity through the martian orbit result in the injection of large amounts of dust

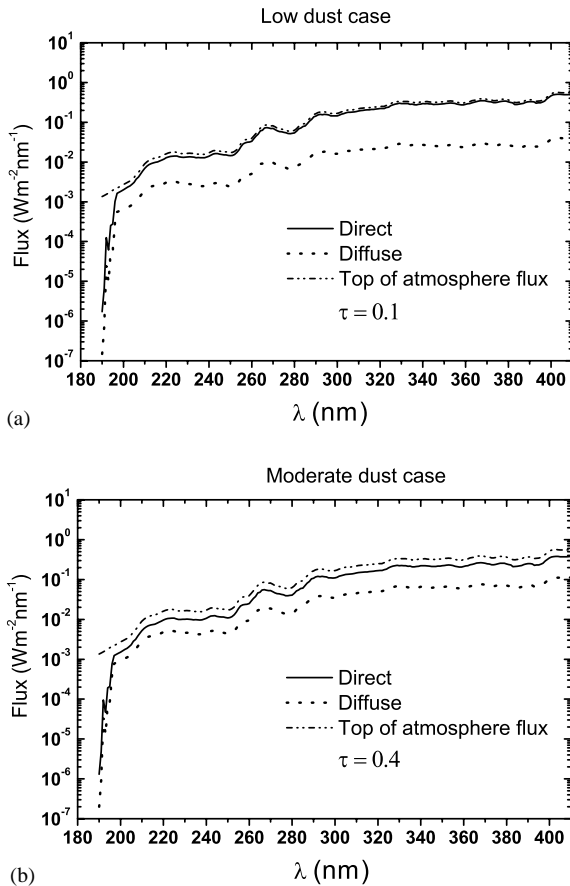


Fig. 4. Two cases during northern summer are shown here for the low dust case, at $L_s = 70^\circ$, latitude = 0° , local noon: (a) shows the case of the lower dust limit, $\tau=0.1$. There is little modification of the input flux, except for the characteristic cutoff near 190 nm; (b) shows the upper limit for this period, with $\tau = 0.4$. There is still little change to the flux, but in comparison to (a) there is a greater difference between direct and diffuse fluxes.

into the atmosphere, significantly altering aerosol column densities. The large-scale (global) dust storms tend to trigger in the southern hemisphere towards perihelion, reaching optical depths in excess of 4 (Pollack et al., 1979). Shown in Fig. 5 are transmission curves for various cases of dust loading during typical dusty southern summers.

It can easily be seen that the presence of large amounts of dust inverts the ratio of direct to diffuse illumination. A reversal of the dominant flux component is seen to occur, and for this particular case it occurs at an optical depth value of 1.4 where the direct and diffuse components become equal. Indeed, the direct component is attenuated at an extremely fast rate with increasing dust loading due to the nature of its exponential dependence, whereas the diffuse component still provides a small but significant contribution even at extremely high dust levels. Variation between aphelion and perihelion was also investigated. Despite the $\sim 40\%$ variation in insolation with orbital position, the surface flux for an equatorial point (0°N) in the lower limiting dust case shows only around 4% variation in total dose between

aphelion and perihelion ($L_s = 250^\circ$ and 70°). Perihelion has a significantly higher incoming flux than aphelion, but this is counteracted by the higher dust activity which increases the lower limiting dust optical depth to 0.5. This causes a corresponding decrease in flux that brings the surface irradiance almost equal to the aphelion case. This effect however no longer applies at points away from the equator, where increased zenith angle with season dominates the absorption effects, causing significant variation in total flux. The same comparison as above for a latitude of 20°S yields a far higher variation in surface flux of $\sim 50\%$ between perihelion and aphelion.

Flux calculations for this case of large amounts of lofted dust should however be considered as an upper limit. This is because the high winds which trigger and perpetuate major dust storms have the effect of lifting a wider range of dust particle sizes, introducing larger particles (when compared to the ‘background’ dust haze) into the atmosphere altering the size distribution of suspended particles. This change in suspended particle size distribution leads to a corresponding change in single-scattering properties of the dust haze, affecting the transmission of solar radiation. For example, the presence of larger suspended particles has the effect of reducing the single-scattering albedo which reduces the total surface UV flux in this case. Here a 20% reduction in ω_{eff} resulted in a 6% reduction of the total UV flux. It is for this reason the flux values quoted here for high dust loading cases should therefore be regarded as an upper limit.

3.2. Diurnal variations

The variation of surface flux can also be studied as a function of local time to recreate the diurnal variations expected at the surface of Mars. Profiles are presented in Fig. 6 for both high and low dust cases, showing direct and diffuse components. The abundance of aerosols through the day is assumed constant here, ignoring effects such as possible ground fogs identified by Pollack et al. (1977) which increase morning optical depths by small amounts. The transmission values therefore should be regarded here as a maximum for the morning period.

The variation through the day shows a symmetric behaviour as expected. An interesting feature is the transition point occurring near sunrise and sunset between direct and diffuse illumination. For relatively low optical depths, the direct signal dominates for the majority of the day, as expected. However, for approximately the first and last 1.5 h of daytime, the diffuse irradiance dominates for any optical depth. This can be explained by consideration of airmass during those times—close to sunrise and sunset, the solar zenith angle is extremely large forcing the incoming flux to traverse a far larger distance through the atmosphere than at later times when the solar zenith angle decreases. The large airmass attenuates the direct flux rapidly due to the Beer’s Law relationship described previously. The diffusive

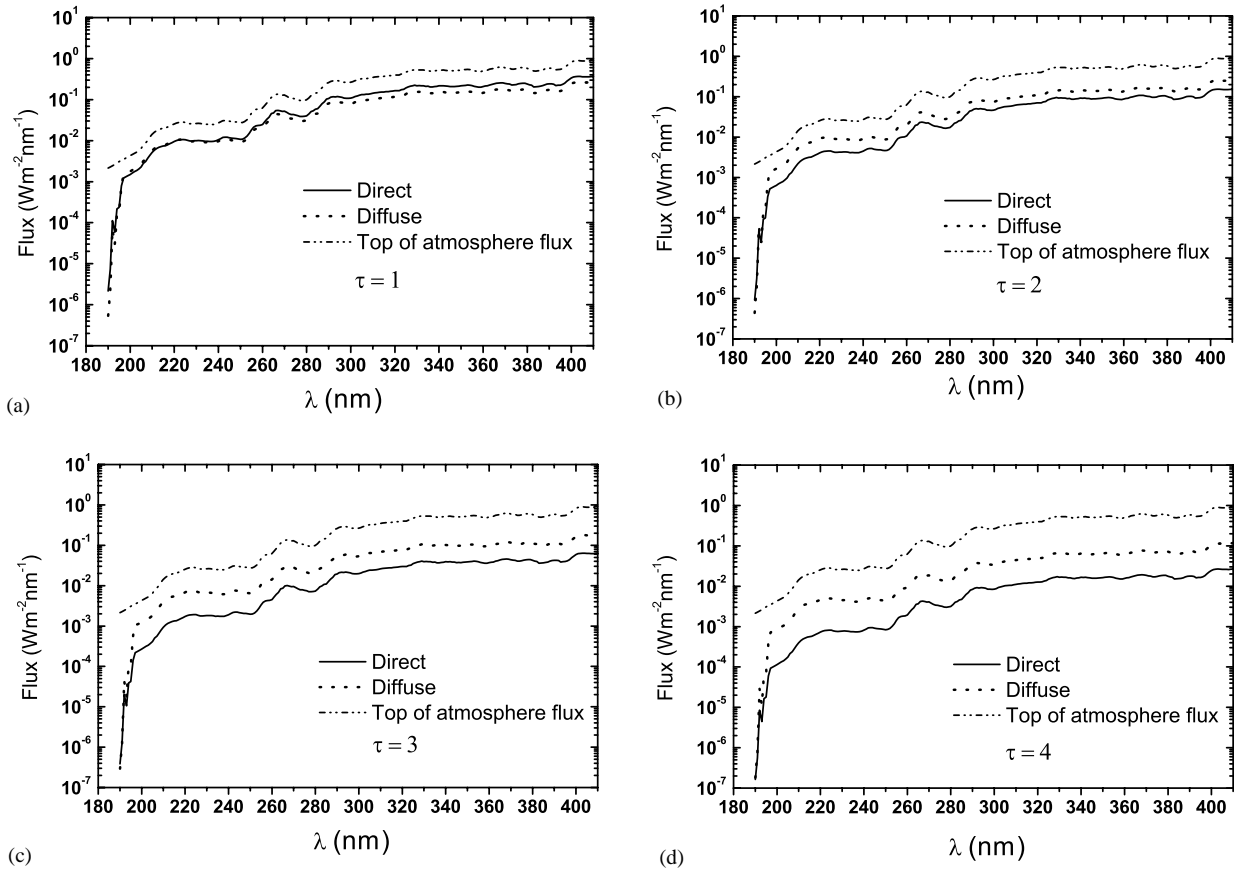


Fig. 5. High dust loading situations are shown here towards perihelion ($L_s = 250^\circ$) for a latitude 20°S at local noon. (a), (b), (c) and (d) show the surface diffuse and direct irradiance for optical depth cases of $\tau = 1, 2, 3$ and 4 , respectively.

scattering effects of the airmass however, are not reduced quite so rapidly here (analogous to the case of high aerosol optical depth) and therefore diffuse illumination dominates for that portion of the day. Also as expected, the same reversal of dominant component occurs as in the previous section, with direct flux dominant in low dust cases and diffuse flux dominant in the high dust case.

3.3. High ozone case

O_3 was first detected in the martian atmosphere by [Barth and Hord \(1971\)](#) using Mariner 7 data. However, O_3 concentration is a seasonally and spatially varying constituent of the martian atmosphere, with results from [Barth et al. \(1973\)](#) indicating that significant O_3 concentrations of up to $1.5 \times 10^{17} \text{ cm}^{-2}$ (5.7 Dobson units (DU)) only occur at high latitudes towards northern winter, declining sharply towards spring (1 DU is the thickness, in units of hundredths of a millimetre, that the total O_3 column would occupy at 0°C and atmospheric pressure. The Earth's ozone layer corresponds to 300 DU, typically). Further work by [Clancy et al. \(1996\)](#) using the HST Faint Object Spectrograph showed results in agreement with this work, improving on the lower detection limit of the Mariner 9 instrument to measure the presence

of small amounts of O_3 at low latitudes ($8.3 \times 10^{15} \text{ cm}^{-2}$ or 0.3 DU) towards aphelion. The presence and disappearance of O_3 can be explained through photochemical interactions with H_2O with which it is anti-correlated in abundance, since photochemical products from the breakdown of H_2O are involved in the catalytic destruction of O_3 in the atmosphere. During northern winter, the formation of the northern water-ice polar cap removes water vapour from the atmosphere, allowing the formation of O_3 through photolysis of CO_2 and reaction of atomic oxygen and O_2 . Thus O_3 abundance reaches a maximum towards northern winter, and begin to fall during spring as the northern polar cap begins to recede, releasing trapped water vapour which in turn begins the photolytic destruction of O_3 . Fig. 7 shows the effect of O_3 on the UV spectrum in typical conditions, with significant absorption seen centred around 250 nm in the UV-C region. This region is the biologically damaging part which is screened out in the terrestrial case by the relatively thick ozone layer. Short-wavelength electromagnetic radiation can have a detrimental effect on many biological systems causing cell destruction, mutagenic changes in the genotype and carcinogenic effects ([Peak and Peak, 1995](#)). The biological response of organisms is highly wavelength-dependent. DNA for example, has a peak absorption near 260 nm which

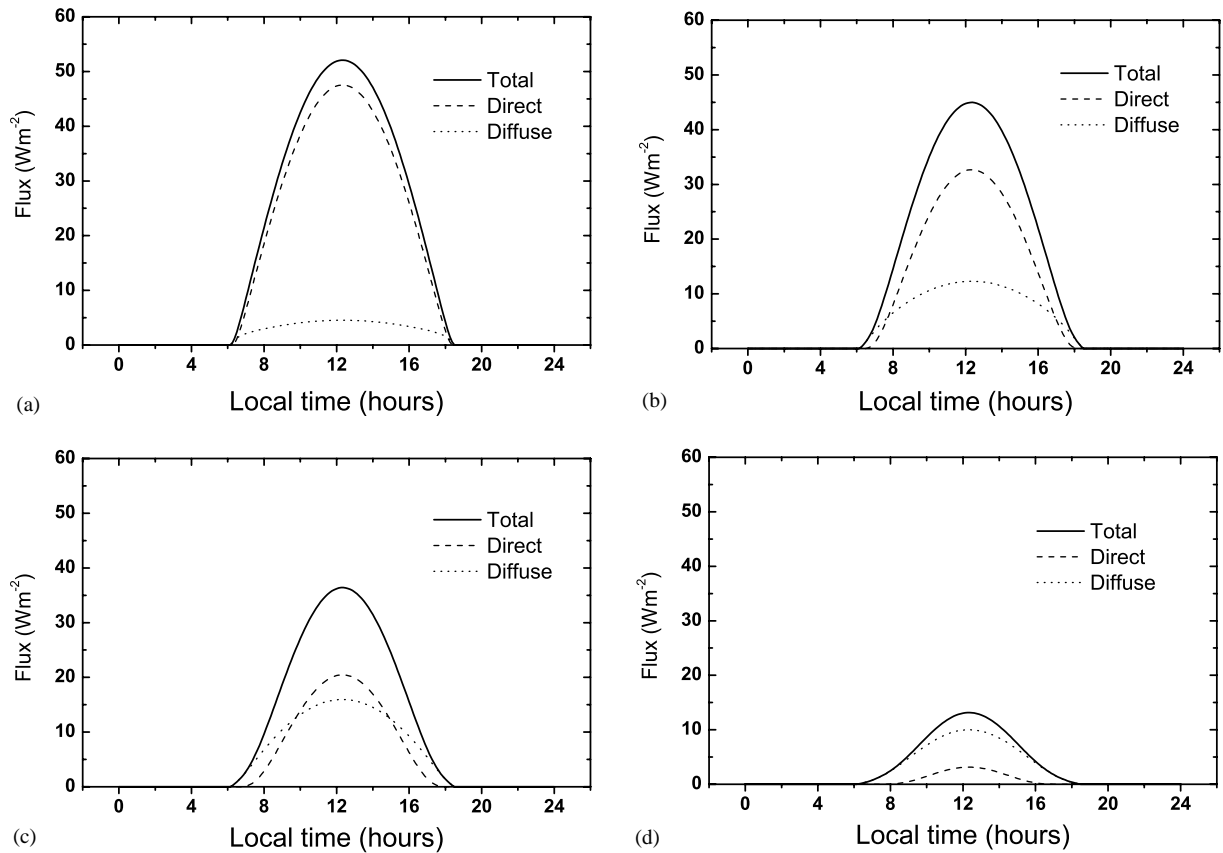


Fig. 6. Diurnal variations for a typical equatorial region near perihelion ($L_s = 250^\circ$) are shown here for different dust levels. (a), (b), (c) and (d), show the flux levels for optical depths of 0.1, 0.5, 1 and 3, respectively. The flux shown is the total UV flux between 190 and 400 nm.

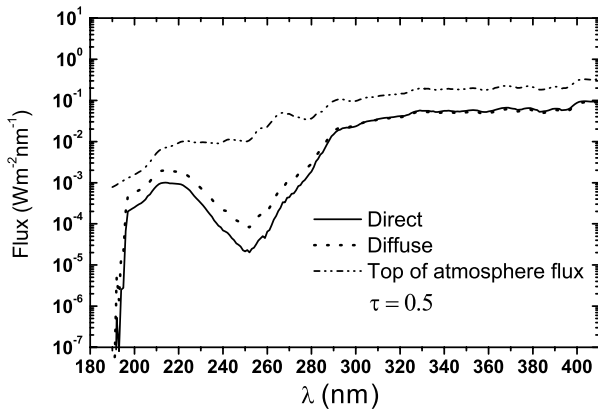


Fig. 7. The effect of O_3 on the UV spectrum is highlighted here, for $L_s = 250^\circ$, latitude = 45°N at local noon with a typical dust loading for northern winter of $\tau = 0.5$ and shows the case with the maximum detected Mariner 9 O_3 abundance of $1.57 \times 10^{17} \text{ cm}^{-2}$ (5.8 DU).

decreases by a factor of six towards 290 nm (the response of various biological organisms are each unique, DNA is shown as an example). Photons at these wavelengths can be directly absorbed by the DNA formation resulting in detrimental modification of the structure most commonly by dimerisation between base pairs. The absorption of most

biological structures sharply increases in the UV-C region below 280 nm coincident with the O_3 absorption band, making them extremely prone to irradiation at these wavelengths. O_3 presence on Mars, though lower by a factor of approximately 300 when compared to Earth, could still offer partial protection for microorganisms on the surface of Mars. However, the presence of a second DNA absorption peak at 220 nm near the edge of the Hartley band means damage would still be incurred to exposed organisms—the relatively low O_3 concentrations result in significant absorption only towards the centre of the absorption band. Also, the variation of significant O_3 abundance limits this possible partial biological protection to northern winter at high latitudes only. Thus, geographical constraints and the presence of the secondary DNA absorption band effectively limit the degree of O_3 protection encountered.

4. Experimental investigation

4.1. Beagle 2 UV sensor

Beagle 2 (B2) is a 30 kg lander set to land on the martian surface in 2003, journeying to Mars onboard the ESA Mars Express spacecraft (Sims et al., 1999). Its primary

Table 3
Instrument details and mass breakdown of the Beagle 2 Environmental Sensor Suite (ESS)

ESS sensor	Description	Mass (g)
UV sensor	200–400 nm	19
Oxidant sensor	Overall oxidation potential	30
Air temp. sensor	Local temp. to 0.5 K accuracy	6
Air pressure sensor	Local pressure to 0.1 mBar accuracy	15
Wind sensor	Speed and direction, temp. sensor included	15
Dust impact detector	Aeolian transport rate	12
Accelerometers	Part of entry and descent landing system	40
Total		137

function is as an exobiology mission lasting a nominal 180 sols, searching for evidence of past life on the martian surface/sub-surface through an array of experiments. One of the instrument packages is the Environmental Sensor Suite (ESS), a collection of instruments designed to monitor the local environment. The package consists of seven separate instruments, with a total mass of 137 g. The mass budget required all instruments to be miniaturised, using commercial microtechnology wherever possible. The instrument list and mass breakdown is given in Table 3.

The UV sensor is designed to monitor the local UV environment of the lander between 200 and 400 nm. The main objective of this instrument is to record directly the previously unmeasured martian flux at the surface and describe this environment from a biological perspective. As mentioned previously, martian flux is a primary consideration in the mutagenesis and survival of organisms at the martian surface—an accurate knowledge of the martian UV-C flux below 280 nm will help quantify the irradiating conditions that would be experienced by any possible martian surface microorganisms. Secondary objectives include studying the nature of interaction between atmospheric dust and incoming solar UV. The presence of dust in the atmosphere and its UV attenuation effects has also yet to be experimentally investigated directly from the surface. Previous in situ dust optical properties investigations from the Viking landers (Pollack et al., 1977) and Pathfinder imaging instruments (Tomasko et al., 1999; Markiewicz et al., 1999) dealt only with the visible and infra-red part of the spectrum. The UV sensor will allow an understanding of the attenuation effects in the ultraviolet, giving a value of optical depth across the 200–400 nm range. The sensor will also be able to measure the transmission effects of any transient phenomenon such as martian dust devils (Ryan and Lucich, 1983). Dust devils are localised vortical columns of air, formed by buoyant thermal plumes created through solar heating of the surface terrain. These columns of air are regarded as an important factor in martian dust transport, picking up

and injecting surface dust into the atmosphere. Pathfinder detected 20 thermal and pressure vortices crossing the lander, and subsequent processing of camera data revealed the presence of dust devil structures in some of the images (Metzger et al., 1999). Analysis of these observed structures gave upper limits of 79 m width, 350 m height, 4.6 m s^{-1} speed and dust loading of $7 \times 10^{-5} \text{ kg m}^{-3}$. The crossing of these transient phenomena over the lander will create a momentary increase in optical depth through the line of sight of the sensor, directly related to the dust loading of the dust devil. Here, the UV sensor will work in conjunction with the other meteorology sensors to categorise fully the physical characteristics of the dust devil.

4.2. UV sensor design

The sensor array sits within the lander body, with a clear view of the martian sky. During operation, the unit requires only 30 mW with six analogue output channels. The low power consumption results in the possibility of continuous operation of the sensor throughout the mission lifetime, as with the rest of the ESS instruments. Sensors sample at a constant low rate (one sample every 0.2 h), but retain the capability to trigger off various instruments into a high sampling rate mode (currently 4 Hz) if any measured values exceed a predefined threshold, i.e. a sudden pressure drop in the case of a dust devil crossing. The sensor head and front end electronics are all mounted on a single printed circuit board and have a total mass of 19 g. Space limitations forced miniaturisation and packing of components into an extremely small area. The total area of the sensor board amounts to 20.1 cm^2 .

The final design consists of an array of six photodiodes with selectively chosen filters to yield a five point spectrum across the UV range, with one broad-band channel. Silicon carbide diodes were chosen for their exceptional dark current characteristics, an important factor considering the expected low fluxes described below. The diodes are naturally radiation hard, a requirement for prolonged operation on the harsh martian surface where the thin atmosphere does not completely block high energy solar and galactic radiation as on Earth. Also, the diodes are blind to wavelengths greater than 400 nm eliminating the need for filters which specifically block the high visible flux which could easily saturate any UV flux. Custom built bandpass filters are incorporated above the sensing diode into industry standard photodiode cans, hermetically sealed from the martian atmosphere. The six channels are arranged to give complete coverage over the modelled UV range, with filter wavelengths and bandwidths for each channel shown in Table 4. The 350 and 300 nm channels are both commercially available devices (Laser Components UK) with integrated filters. Both incorporate broad-band filters, chosen since the variation in flux with wavelength in this region of the spectrum is minimal. The lack of features in these bands allow the use

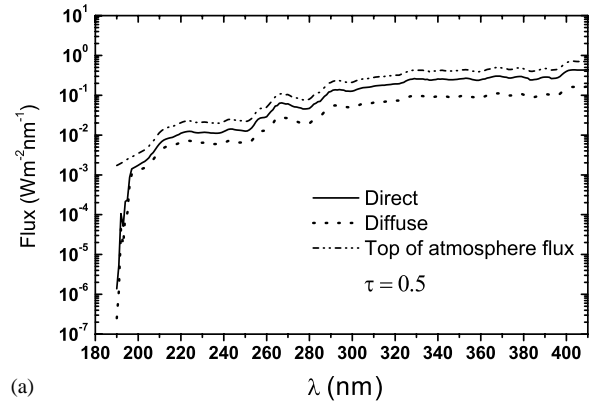
Table 4

UV sensor channels: filter centre wavelengths (CWL) and full-width half-maximum bandwidths (FWHM). Also shown is the expected accuracy and resolution of each channel

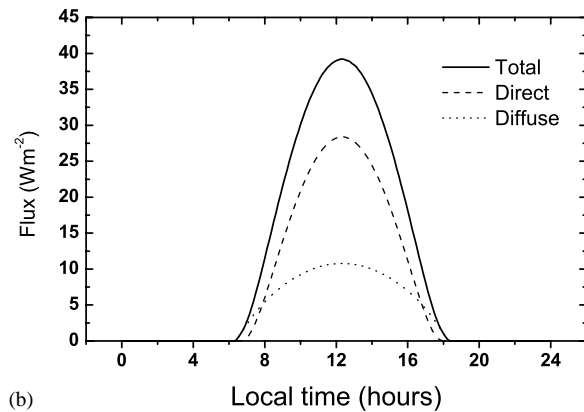
Filter CWL (nm)	FWHM (nm)	Accuracy (W m^{-2})	Resolution (W m^{-2})
210	20	3.5×10^{-11}	9.0×10^{-12}
230	11	4.0×10^{-11}	9.5×10^{-12}
250	18	9.0×10^{-11}	2.0×10^{-11}
300	35	1.5×10^{-9}	3.8×10^{-10}
350	65	5.0×10^{-9}	1.2×10^{-9}
Full range 200–400	n/a	8.5×10^{-9}	2.0×10^{-9}

of broad-band filters to give an averaged flux level, which can then be deconvoluted back to the spectral curve for that particular region using the model presented here. Three other channels utilise custom-made narrow bandpass filters (Barr Associates Inc.) to monitor features in the UV-C region, spread throughout the short-wave region to give even coverage. The 250 nm channel is placed directly in the O_3 absorption band, though this is unlikely to be observed at the Beagle 2 landing site which is too close to the equator (10°N) for the formation of any significant O_3 concentrations. The positions of the 210, 230 and 250 nm channels were set by the possibility of weak absorption bands of the martian dust. TiO_2 was proposed by Pang and Ajello (1977) as a possible UV-absorbing component of airborne dust, through analysis of Mariner 9 ultraviolet spectra. This aspect was investigated by Nansheng and Minji (1983), and TiO_2 (in the anatase phase) does appear to possess the optical properties to be consistent with the modelled absorption indices from Mariner 9 data and has also been identified as present in small amounts ($\sim 1\%$) in the martian soil from Pathfinder results (Bell III et al., 2000). TiO_2 is opaque in the UV possessing a main absorption band centred at 210 nm, with secondary bands at 230 and 250 nm. Hence, on the basis of the possible presence of TiO_2 in the airborne martian dust, these centre wavelengths were chosen for the three short wave channels. The final channel is open to the entire UV range 200–400 nm (no filter). This channel will monitor the total UV flux and aid in accurate verification of the model to assist in deconvolution of the five point measured spectrum back to a spectral curve (with reference optical depth being provided by the lander cameras). It will also by virtue of absence, give a rough indication of the degree of darkening of the filters used in the other channels over the mission lifetime as they are exposed to a prolonged UV dose. A marked decrease in signal over time from the five filtered channels but not the open channel, would be indicative of this effect.

The model presented here was used to define the UV environment that Beagle 2 is expected to encounter. Flux levels were calculated for a theoretical maximum flux scenario during the nominal mission lifetime, and these values were used to set the gain of each channel to avoid possible satu-



(a)



(b)

Fig. 8. The Beagle 2 landing site UV environment: (a) shows the spectrum of the expected flux at local noon and (b) shows the diurnal variations to be encountered.

ration. Beagle 2 will land at $L_s = 322^\circ$ at a nominal 10°N in the Isidis region, midway between northern winter and spring. This time is towards the end of the period of high dust activity in the southern hemisphere, with optical depths ranging from 0.5 to occasionally in excess of 4. For a maximum exposure case, an optical depth value of 0.5 was used. With the maximum exposure values set, the theoretical accuracy and resolution of each channel were defined, given in Table 4. Fig. 8 shows the expected UV spectrum for the Beagle 2 landing site at the beginning of the mission, along with the diurnal variation. It can be seen that the UV-C component of the spectrum becomes increasing weaker towards the 210 nm channel, making the need for a low dark current detector paramount.

5. Conclusion

Using the model presented here, it has been possible to characterise the surface UV environment for a variety of cases. The model takes full account of all the important martian atmospheric gases and also the presence of suspended dust, but does not consider any ice hazes formed in the atmosphere. The radiative transfer approximation method

employed here allows for fast and easy computation of many known martian surface conditions, yielding results on surface irradiance in terms of both direct and diffuse components. Latitudinal variations observed include a distinct increase in the diffuse component with increasing latitude, as the air mass scattering effect becomes more dominant. The same effect is seen in diurnal variations at any point, with transmission at large zenith angles close to sunrise and sunset being almost completely diffuse in nature, as intuitively expected. O₃ concentrations at high latitudes towards northern winter are also shown to have a partial shielding effect in the biologically damaging UV-C region, though some shorter wavelengths do penetrate. Minimal effects are seen for low dust cases, except for the characteristic CO₂ cutoff seen in all situations. High dust cases have the effect of reducing the direct input to negligible levels, though a significant irradiance is still provided through diffuse scattering from atmospheric dust.

Development of the model also assisted in design of the UV sensor onboard Beagle 2 for monitoring of the local martian environment. Spectral curves of expected conditions aided in the selection of which regions in the UV to study, namely broad filters for the plateau regions 280–400 nm, with narrow band filters monitoring the more variable 200–280 nm region centred around possible TiO₂ absorption bands. The model was then used to set gain characteristics for each channel. Further work will concentrate on the use of the model to characterise fully and simulate the Beagle 2 UV sensor outputs in terms of all expected phenomena throughout the mission lifetime.

Acknowledgements

The lead author would like to thank Martin Towner (B2 ESS Project Manager) and Mark Sims (B2 ESS PI) for continued assistance with the Beagle 2 UV sensor. Thanks are also extended to Charles Cockell for helpful counsel, and Chris Varney of Laser Components UK for his keen interest and assistance in the production of the UV sensor heads. David Catling was supported by the University of Washington's "University Initiatives Fund" (UIF) in Astrobiology. The lead author also gratefully acknowledges studentship funding from PPARC to carry out this research as part of a Ph.D. project.

References

- Amoruso, A., Crescentini, L., Silvia Cola, M., Fiocco, G., 1996. Oxygen absorption cross-section in the Herzberg continuum. *J. Quant. Spectrosc. Radiat. Transfer* 56 (1), 145–152.
- Barth, C.A., Hord, C.W., 1971. Mariner 7 ultraviolet spectrometer: topography and polar cap. *Science* 173, 197–201.
- Barth, C.A., Hord, C.W., Stewart, A.I., Lane, A.L., Dick, M.L., Anderson, G.P., 1973. Mariner 9 ultraviolet spectrometer experiment: seasonal variation of ozone on Mars. *Science* 179, 795–796.
- Bell III, J.F., McSween Jr., H.Y., Crisp, J.A., Morris, R.V., Murchie, S.L., Bridges, N.T., Johnson, J.R., Britt, D.T., Golombek, M.P., Moore, H.J., Gosh, A., Bishop, J.L., Anderson, R.C., Bruckner, J., Economou, T., Greenwood, J.P., Gunnlaugsson, H.P., Hargraves, R.M., Hviid, S., Knudsen, J.M., Madsen, M.B., Reid, R., Reider, R., Soderblom, L., 2000. Mineralogic and compositional properties of martian soil and dust: results from Mars Pathfinder. *J. Geophys. Res.* 105 (E1), 1721–1755.
- Cebula, R.P., Thuillier, G.O., Vanhoosier, M.E., Hilsenrath, E., Herse, M., Brueckner, G.E., Simon, P.C., 1996. Observations of the solar irradiance in the 200–350 nm interval during the ATLAS 1 mission: a comparison among three sets of measurements—SSBUV, SOLSPEC, and SUSIM. *Geophys. Res. Lett.* 23 (17), 2289.
- Chylek, P., Grams, G.W., 1978. Scattering by nonspherical particles and optical properties of martian dust. *Icarus* 36, 198–203.
- Clancy, R.T., Wolff, M.J., James, P.B., Smith, E., Billawala, Y.N., Lee, S.W., Callan, M., 1996. Mars ozone measurements near the 1995 aphelion: Hubble space telescope ultraviolet spectroscopy with the faint object spectrograph. *J. Geophys. Res.* 101 (E5), 12,777–12,783.
- Cockell, C.S., Catling, D.C., Davis, W.L., Snook, K., Kepner, R.L., Lee, P., McKay, C.P., 2000. The ultraviolet environment of Mars: biological implications past, present and future. *Icarus* 146, 343–359.
- Floyd, L.E., Prinz, D.K., Crane, P.C., Herring, L.C., Brueckner, G.E., 1999. SUSIM UARS measurements of solar UV irradiance. *Adv. Space Res.* 24 (2), 225–228.
- Haberle, R.M., McKay, C.P., Pollack, J.B., Gwynne, O.E., Atkinson, D.H., Appelbaum, J., Landis, G.A., Zurek, R.W., Flood, D.J., 1993. Atmospheric effects on the utility of solar power on Mars. In: Lewis, J.S., Matthews, M.S., Guerrieri, M.L. (Eds.), *Resources of Near-Earth Space*. University of Arizona Press, Tucson, pp. 845–885.
- Horneck, G., 1993. Responses of *Bacillus subtilis* spores to space environment: results from experiments in space. *Origins Life Evol. Biosphere* 23, 37–52.
- James, P.B., Clancy, R.T., Lee, S.W., Martin, L.J., Singer, R.B., Smith, E., Kahn, R.A., Zurek, R.W., 1994. Monitoring Mars with the Hubble space telescope: 1990–1991 observations. *Icarus* 109, 79–101.
- Joseph, J.H., Wiscombe, W.J., Weinman, J.A., 1976. The Delta–Eddington approximation for radiative flux transfer. *J. Atmos. Sci.* 33, 2452–2459.
- Kuhn, W.R., Atreya, S.K., 1979. Solar radiation incident on the surface of Mars. *J. Mol. Evol.* 14, 57–64.
- Lewis, B.R., Carver, J.H., 1983. Temperature dependence of the carbon dioxide photoabsorption cross section between 1200 and 1970 Å. *J. Quant. Spectrosc. Radiat. Transfer* 30 (4), 297–309.
- Lodders, K., Fegley Jr., B., 1998. *The Planetary Scientist's Companion*. Oxford University Press, New York.
- Malicet, J., Daumont, D., Charbonnier, J., Parisse, C., Chakir, A., Brion, J., 1995. Ozone UV spectroscopy II: absorption cross sections and temperature dependence. *J. Atmos. Chem.* 21, 263–273.
- Mancinelli, R.L., Klovstad, M., 2000. Martian soil and UV radiation: microbial viability assessment on spacecraft surfaces. *Planet. Space Sci.* 48, 1093–1097.
- Markiewicz, W.J., Sablotny, R.M., Keller, H.U., Thomas, N., Titov, D., Smith, P.H., 1999. Optical properties of the Martian aerosols as derived from Imager for Mars Pathfinder midday sky brightness. *J. Geophys. Res.* 104 (E4), 9009–9017.
- Metzger, S.M., Carr, J.R., Johnson, J.R., Parker, T.J., Lemmon, M.T., 1999. Dust devil vortices seen by the Mars Pathfinder camera. *Geophys. Res. Lett.* 26 (18), 2781–2784.
- Moroz, V.I., Petrova, E.V., Ksanfomality, L.V., 1993. Spectrophotometry of Mars in the KRFM experiment of the Phobos 2 mission: some properties of the particles of atmospheric aerosols and the surface. *Planet. Space Sci.* 41 (8), 569–585.
- Nansheng, Z., Minji, L., 1983. Explanation of UV band absorption spectra caused by martian dust cloud in 1971. *Kexue Tongbao* 28 (6), 779–782.

- Ockert-Bell, M.E., Bell III, J.F., Pollack, J.B., McKay, C.P., Forget, F., 1997. Absorption and scattering properties of the martian dust in the solar wavelengths. *J. Geophys. Res.* 102 (E4), 9039–9050.
- Owen, T., 1992. The composition and early history of the atmosphere of Mars. In: Kieffer, H.H., Jackosky, B.M., Snyder, C.W., Matthews, M.S. (Eds.), *Mars*. University of Arizona Press, Tucson, pp. 818–834.
- Owen, T., Sagan, C., 1972. Minor constituents in planetary atmospheres: ultraviolet spectroscopy from the Orbiting Astronomical Observatory. *Icarus* 16, 557–568.
- Pang, K., Ajello, J.M., 1977. Complex refractive index of martian dust: wavelength dependence and composition. *Icarus* 30, 63–74.
- Pang, K., Ajello, J.M., Hord, C.W., Egan, W.G., 1976. Complex refractive index of Martian dust: mariner 9 ultraviolet observations. *Icarus* 27, 55–67.
- Peak, M.J., Peak, J.G., 1995. Photosensitized reactions of DNA. In: Horspool, W.M., Song, P. (Eds.), *CRC Handbook of Organic Photochemistry and Photobiology*. CRC Press, Boca Raton, FL, pp. 1318–1325.
- Pollack, J.B., Colburn, D., Kahn, R., Hunter, J., Van Camp, W., Carlston, C.E., Wolf, M.R., 1977. Properties of aerosols in the martian atmosphere, as inferred from Viking lander imaging data. *J. Geophys. Res.* 82 (28), 4479–4496.
- Pollack, J.B., Colburn, D.S., Michael Flaser, F., Kahn, R., Carlston, C.E., Pidek, D., 1979. Properties and effects of dust particles suspended in the martian atmosphere. *J. Geophys. Res.* 84 (B6), 2929–2945.
- Pollack, J.B., Ockert-Bell, M.E., Shepard, M.K., 1995. Viking lander image analysis of Martian atmospheric dust. *J. Geophys. Res.* 100 (E3), 5235–5250.
- Ryan, J.A., Lucich, R.D., 1983. Possible dust devils, vortices on Mars. *J. Geophys. Res.* 88 (C15), 11005–11011.
- Sagan, C., Pollack, J.B., 1974. Differential transmission of sunlight on Mars: biological implications. *Icarus* 21, 490–495.
- Sims, M.R., Pillinger, C.T., Wright, I.P., Dowson, J., Whitehead, S., Wells, A., Spragg, J.E., Fraser, G., Richter, L., Hamacher, H., Johnstone, A., Meredith, N.P., de La Nougerede, C., Hancock, B., Turner, R., Peskett, S., Brack, A., Hobbs, J., Newns Sr., M., 1999. Beagle 2: a proposed exobiology lander for ESA's 2003 Mars express mission. *Adv. Space Res.* 23 (11), 1925–1928.
- Toigo, A.D., Richardson, M.I., 2000. Seasonal variation of aerosols in the martian atmosphere. *J. Geophys. Res.* 105 (E2), 4109–4121.
- Tomasko, M.G., Doose, L.R., Lemmon, M., Smith, P.H., Wegryn, E., 1999. Properties of dust in the martian atmosphere from the Imager on Mars Pathfinder. *J. Geophys. Res.* 104 (E4), 8987–9007.
- Wolff, M.J., Lee, S.W., Clancy, R.T., Martin, L.J., Bell III, J.F., James, P.B., 1997. 1995 observations of Martian dust storms using the Hubble Space Telescope. *J. Geophys. Res.* 102 (E1), 1679–1692.
- Wuttke, M.W., Keller, H.U., Markiewicz, W.J., Petrova, E., Richter, K., Thomas, N., 1997. Properties of dust in the martian atmosphere: a revised analysis of Phobos/KRFM data. *Planet. Space Sci.* 45 (3), 281–288.
- Zureck, R.W., 1978. Solar heating of the martian dusty atmosphere. *Icarus* 35, 196–208.